www.czasopisma.pan.pl PAN POLSKA AKADEMIA NAUK www.journals.pan.pl

Arch. Metall. Mater. **68** (2023), 3, 1017-1023

DOI: https://doi.org/10.24425/amm.2023.145469

M. ŠOFER[1*], P. KWIATOŃ[2], P. PAVLÍČEK[1]

APPLICATION OF IMPROVED b-VALUE AND CLUSTERING ANALYSIS FOR STRUCTURAL INTEGRITY ASSESSMENT OF CFRP SPECIMEN UNDER TENSILE LOADING

In the present study, the evolution of different failure mechanisms in carbon fiber reinforced polymer composites is being investigated using acoustic emission technique, unsupervised clustering technique and improved b-value analysis. The experimental part involved the realization of tensile tests of different materials, namely samples with $[0/90]_{2S}$ uniaxial layer configuration and $[0/90]_{2S}$ twill fabric samples. Both types of tests were monitored using one wideband acoustic emission sensor, while the tensile tests of twill fabric samples were additionally supplemented with resonant acoustic emission sensor to perform a comparative analysis between datasets from resonant/wideband acoustic emission sensor. The comparative study itself was preceded by the failure mechanisms characterization process, which has been performed on the tensile test dataset of $[0/90]_{2S}$ layer configuration with the contribution of clustering technique. The subsequent analysis of the twill fabric resonant/wideband acoustic emission sensor datasets included the improved b-value technique, which relates the magnitude of fracture with the slope of the amplitude distribution. The presented results, especially in terms of the improved b-value technique applied to individual clusters, show enhanced ability to assess in more detail the actual structural integrity depending on the applied load.

Keywords: CFRP composite; Acoustic emission; Improved b-value analysis

1. Introduction

Structural integrity monitoring of composite structures is becoming increasingly important due to their more intensive use in many applications for aerospace, automotive, or medical sectors, where Carbon Fiber Reinforced Polymer (CFRP) composites are being extensively involved. Their main benefit is chemical resistivity, very high strength/weight ratio, corrosion resistance, low coefficient of thermal expansion or the ability to tailor the composite layout to a specific application [1]. However, the main drawback of these materials is the complex nature of failure mechanisms including brittle-like failure manner [2]. This fact thus places complex demands on the methodology for assessing the structural integrity of components made of composite materials.

One of the very specific non-destructive (NDT) methods, used among other things for the above purposes, is the acoustic emission (AE) method. This NDT method is based on the detection of acoustic stress waves, resulting from a sudden stress redistribution owing to structural damage in micro/macro scale [3]. The given method also supports localization of the AE sources using an array of sensors, which is a significant benefit for many industrial applications, where we encounter thin-walled geometries. The plate-like character enables the transformation of the initial voluminal waves into Rayleigh or Lamb guided waves [4,5], which exhibit dispersion [6,7] and thus the AE signal processing methodology is an integral part of the measurement procedure.

The above-mentioned complexity of composite failure mechanisms has led a number of researchers to propose different types of structural integrity assessment methodologies such as parameter-based analysis [8], signal-based analysis [9] or procedures using supervised/unsupervised pattern recognition approach [10,11]. In addition to the above types of analyses, it is possible to come across those that use only one parameter for their operation, namely the AE signal amplitude. B-value analysis [12], or its derivative called improved b-value analysis (Ib) [13] has its origin in Gutenberg-Richter relationship [14], commonly used in seismology. The Ib/b-value parameter is being calculated from the logarithmized amplitude distribution of AE signals, which otherwise exhibit a power-law distribution in linear scale.

[1] VŠB-TECHNICAL UNIVERSITY OF OSTRAVA, FACULTY OF MECHANICAL ENGINEERING, DEPARTMENT OF APPLIED MECHANICS, 17. LISTOPADU 15/2127, 708 33 OSTRAVA-PORUBA, CZECH REPUBLIC
[2] CZESTOCHOWA UNIVERSITY OF TECHNOLOGY, FACULTY OF MECHANICAL ENGINEERING AND COMPUTER SCIENCE, DEPARTMENT OF MECHANICS AND MACHINE DESIGN FUNDAMENTALS, 73 DĄBROWSKIEGO STR., 42-201 CZĘSTOCHOWA, POLAND

* Corresponding author: michal.sofer@vsb.cz

In this paper, we introduce a case focused on the application of both the Ib value analysis and the combination of Ib value analysis and clustering technique on the tensile test results of CFRP $[0/90]_{2S}$ twill fabric samples. Part of the methodology is the implementation of a series of tensile tests of $[0/90]_{2S}$ layer configuration CFRP samples supplemented by AE monitoring using a wideband sensor, which was used to characterize the individual damage mechanisms. In the next step, tensile tests of the twill fabric specimens were performed, where the monitoring of AE was provided using resonant and wideband AE sensors. Both datasets subsequently underwent Ib value analysis, with the difference that in the case of wideband AE sensor dataset, the given method was additionally applied to the manually clustered data using the peak frequency. The overall analysis of both datasets points to the advantage of a generally comprehensive overview, which is provided by a combination of single-parameter failure mechanism characterization and Ib value analysis.

2. Experiments

The experimental part involved two series of tensile tests, namely a series of three specimens with $[0/90]_{2S}$ uniaxial layer configuration (T1 samples) and a series of three twill fabric specimens also with $[0/90]_{2S}$ configuration (T2 samples). The T1 samples were made of high-performance carbon/epoxy prepreg CM-Preg T-C-230/600 CP004 39 with a nominal ply thickness of 0.25 mm, while the production process of the T2 samples included LH 289 epoxy resin with curing agent H146 and $[0/90]_{2S}$ 600g/m^2 twill fabric (Havel Composites CZ Company Ltd., Czech Republic). TABLE 1 and Fig. 1 respectively present detailed information related to the dimensions of the samples as well as their stacking sequence. Both test series have been conducted on Testometric M500-50CT (50 kN load cell, accuracy: +/–0.5% of the load cell capacity) universal testing machine in deformation-controlled mode with an upper grip speed of 1 mm/min.

TABLE 1

Characterisation of the test specimens

Label/Number of specimens	Stacking sequence	Thickness [mm]
T1/3	$(90°, 0°)_{4S}$	2
T2/3	$(90°, 0°)_{7}$	5

At this point it is necessary to state the reasons why the clustering analysis itself was not applied to T2 samples and instead the given process was preceded by the characterization of individual damage mechanisms on T1 samples:

1. The implementation of tensile tests of T1 samples is part of a larger study focusing on a complex process of failure mechanisms characterization in the case of CFRP composites. The study involves realization of tensile/compact tension tests of unidirectional and cross-ply specimens.

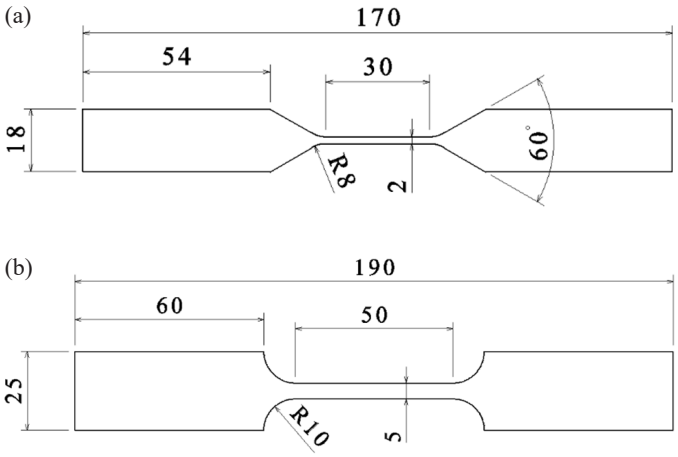

Fig. 1. Geometry of the tested specimens: (a) T1 sample; (b) T2 sample

2. The stacking sequence of T2 samples including the density of the used twill fabric predetermines the given samples for relatively high acoustic emission activity across individual types of mechanisms. The entire management of data preprocessing and their subsequent clustering would therefore be much more time-consuming. If we identify effective indicators for individual failure mechanisms based on point 1, it is possible to perform time-saving filtering and sorting of the AE data.

2.1. Acoustic emission testing

The AE activity has been monitored using Vallen AMSY-6 AE system with incorporated ASIP-2A signal processor card with frequency filter and sampling frequency set to 50-1100 kHz and 5 MHz, respectively. The T1 specimens utilized wideband DWC B454 AE sensor coupled with Vallen AEP5H 40 dB preamplifier, whereas the series of T2 specimens used in addition to the DWC B454 AE sensor also Vallen VS150M resonant sensor coupled with Vallen AEP5H 34 dB preamplifier. The AE hit detection mechanism uses a philosophy of a fixed detection threshold set to 28 dB_{AE} with an active frontend filter ($E_{min} > 10$ aJ). A relatively low threshold value could be set due to the of the background noise RMS value not exceeding 16 and 14 dB_{AE} in the case of Vallen VS150M/Vallen AEP5H 34 dB preamplifier and DWC B454/ Vallen AEP5H 40 dB preamplifier respectively. Possibly occurring low-energy signals originating from the background noise were eliminated by the aforementioned energy filter, the value of which was determined empirically. The Duration Discrimination Time and the Rearm Time, responsible for hit generation and grouping process, were set to 100 µs.

3. Clustering analysis

The characterization of individual damage mechanisms was realized with the use of the unsupervised spectral clustering technique, which is an interesting alternative to k-means [8],

TABLE 2

Characterisation of the involved AE features

Feature	Description
Amplitude	The largest voltage peak of the given AE hit in dB_{AE} (dB rel. to 1 µV before the input to the preamplifier)
Risetime	Time interval in µs between the first threshold crossing and the reached maximum amplitude in µs.
Duration	Time interval in µs between the first and the last threshold crossing in µs.
Energy	Integral of the squared AE signal over time in aJ.
f_p – Peak frequency	Frequency corresponding to the maximum magnitude in the frequency spectrum in kHz.
f_c – Freq. centroid	Centre of mass of the frequency spectrum in kHz.
f_{pw} – Weighted peak frequency	Square root of the product between the peak frequency and frequency centroid in kHz.
RA value	Risetime/peak amplitude ratio (in µs/dB_{AE}).

k-medoid, or fuzzy k-means approaches. A major advantage of this method is its simple implementation including much better performance compared to the classical approaches such as the above-mentioned k-means [15]. The implementation of the method is introduced in [15] or [16].

To get the best possible clustering results, it is necessary to perform an analysis on a predefined group of features (see TABLE 2) from which only the important ones need to be selected. The extraction process of the important features involved Laplacian score (LS) technique introduced by X. He et al in 2005 [17].

The LS technique affiliates to each feature a real number in the range 0 to 1, thus reflecting its locality preserving power. According to the study by Ichenihi et al. [18], the important features can be defined as those having their LS score greater than 0.9. It has to be noted, that both clustering analysis, as well as the LS score computation procedure, have been conducted in MATLAB software.

In addition to the fact that only those features that are marked as important enter the clustering process, it is necessary to assess the optimal number of clusters. For these purposes, we used a metric called the Silhouette Coefficient (SC), which expresses the mean of the Silhouette values over all data points [19]. The Silhouette value $s(i)$ for individual data point x_i within the given dataset is defined as follows:

$$s(i) = \frac{b(x_i) - a(x_i)}{\max\left(a(x_i), b(x_i)\right)} \tag{1}$$

where $a(x_i)$ refers to the average intracluster distance of the point x_i related to all other points within the concerned cluster, while $b(x_i)$ denotes the minimum of the average intercluster distances of the point x_i to all points in each other cluster [20].

4. Improved b-value analysis

The implementation of b-value method can be found most often in a number of applications that have to do with a damage assessment in civil engineering [21,22] or composite science [12,23]. However, the origins of this method are linked with earthquake seismology, where it relates magnitude of the earthquake M with the total number of earthquakes $N(M)$ of magnitude larger than M also known as Gutenberg-Richter relation [12]:

$$\log_{10} N(M) = a - bM \tag{2}$$

$$N(M) = \int_{M}^{\infty} n(M)\, dM \tag{3}$$

where a, b denote empirical constants and $n(M)$ refers to the number of earthquakes of magnitude M. From Eq. (2) is obvious, that the b-value coefficient denotes the negative gradient of the log-linear plot of the event and magnitude and therefore represents the slope of the amplitude distribution [12]. The Gutenberg-Richter formula can be for the purposes of AE technique modified to the following definition:

$$\log_{10} N_{AE} = a - bA_{\mu V} \rightarrow \log_{10} N_{AE} = a - b\frac{A_{dB_{AE}}}{20} \tag{4}$$

where $A_{\mu V}$ denotes the AE event amplitude in μV and $A_{dB_{AE}}$ refers to the amplitude in dB_{AE}. The b-value concept served as a basis for improved b-value method, which incorporates the statistical parameters of the amplitude distribution such as the mean value (μ) and standard deviation (σ) – see Fig. 2 [23].

The slope of the amplitude distribution is then calculated using the following relation:

$$Ib = \frac{\log_{10} N_{AE}\left(\mu - \alpha_1\sigma\right) - \log_{10} N_{AE}\left(\mu + \alpha_2\sigma\right)}{\left(\alpha_1 - \alpha_2\right)\sigma} \tag{5}$$

where α_1, α_2 denote the multiples of standard deviation (in our case set to 1).

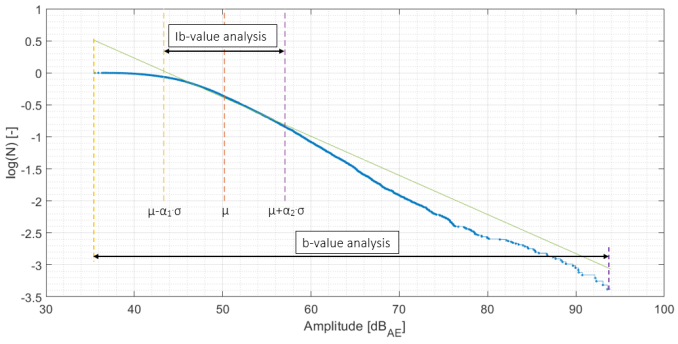

Fig. 2. b-value/improved b-value definition [21]

5. Results and discussion

5.1. Characterization of failure mechanisms

The characterization of failure mechanisms was carried out using the T1 samples dataset, on which Scanning Electron Microscopy (SEM) imaging has been applied in addition to the clustering analysis. Fig. 3 reports four detected microscopic failure mechanisms, namely: fiber failure (Fig. 3b), fiber pull-out (Fig. 3b), fiber/matrix debonding (Fig. 3b) and matrix cracking (Fig. 3c), which subsequently induces delamination (Fig. 3a).

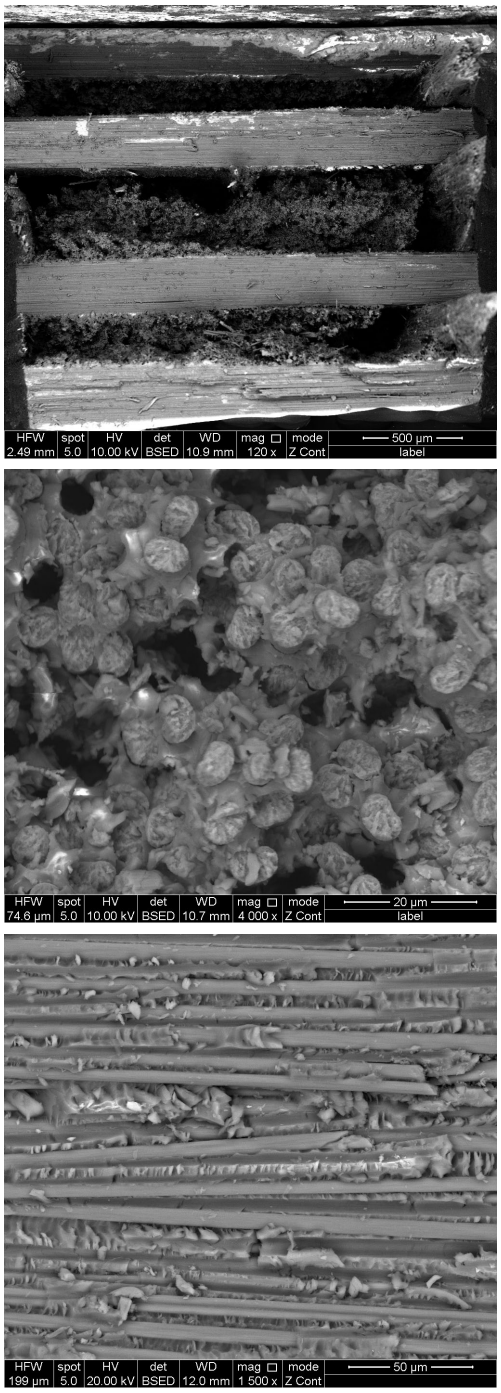

Fig. 3. SEM analysis of T1 specimen: (a) General view including delamination; (b) Fiber failure including fiber pull-out and fiber/matrix debonding; (c) Matrix cracking including fiber/matrix debonding

Let us now return to the clustering process itself, where the important features were selected according to the LS technique and the score value greater than 0.9 (see chapter 3): Weighted peak freq., Peak freq., Amplitude, and Freq. centroid – see Fig. 4. According to the clustering analysis is the optimal number of clusters equal to 3 (SC = 0.722). Fig. 5 displays the already clustered data in the form of Amplitude/Energy versus f_p dependencies.

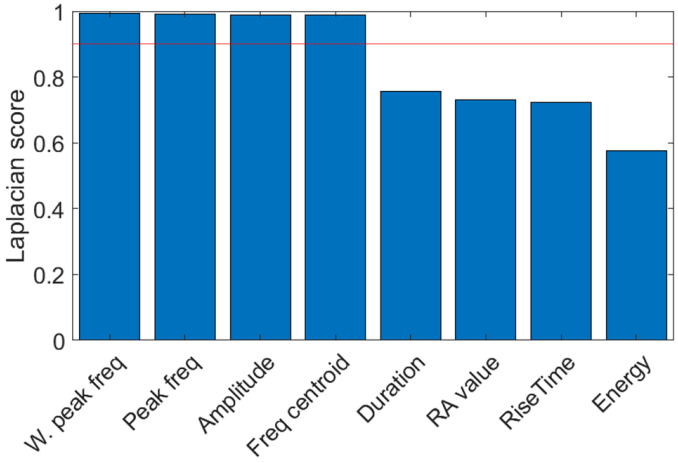

Fig. 4. Results of LS technique

Although, according to the application of the spectral clustering method, clustering into three clusters appears to be optimal, it can be noted that cluster No. 2 consists of two separate clusters. The fact that we did not reach the optimum in the form of four clusters (four reported failure mechanisms in total) is mainly due to the ratio of AE hits in the range of peak frequency 200-400 kHz and 400-600 kHz. Based on our more extensive research activities within this field, which also involved SEM analysis, we have concluded that the general parameter for distinguishing the individual damage mechanisms between each other is the peak frequency. The obtained relation between the given failure mode and peak frequency is summarized in TABLE 3 and is largely consistent with [24].

It is necessary to point out that the mentioned parametric selection in the sense of peak frequency is possible in the given case especially for very small dimensions of the active zone within which the damage process takes place. In the case of real structures, where a much larger distance between the sensor and the potential source of acoustic emission is assumed, it is much more appropriate to choose a derived parameter such as weighted peak frequency (see TABLE 2).

TABLE 3

Failure mechanisms characterization using peak frequency parameter

Failure mechanism	Peak frequency range [kHz]
Matrix cracking/Delamination	50÷200
Debonding	200÷400
Fiber failure	400÷600
Fiber pull-out	>600

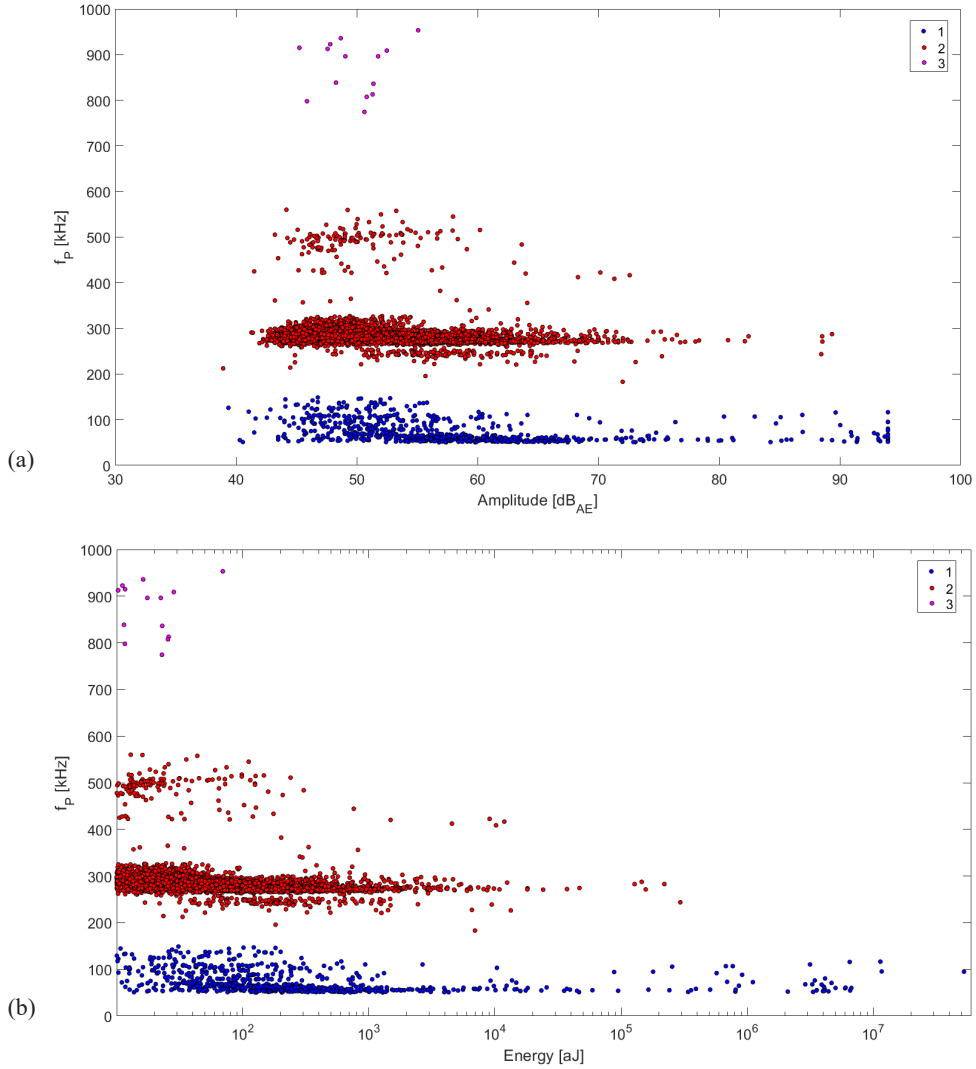

Fig. 5. Results of the clustering analysis: (a) Amplitude versus f_p; (b) Energy versus f_p

5.2. Ib-value analysis of T2 sample series tensile test

The application of the Ib-value analysis to the selected dataset from T2 samples series was of three types:

- Ib-value analysis of VS150M resonant sensor dataset.
- Ib-value analysis of DWC B454 wideband sensor dataset.
- Ib-value analysis of DWC B454 wideband sensor dataset, which has been filtered using the peak frequency ranges (see TABLE 3).

Fig. 6 displays the Ib-value versus upper grip displacement curves for both datasets, i.e. VS150M and DWC B454. The exponent value has been calculated from dataset containing

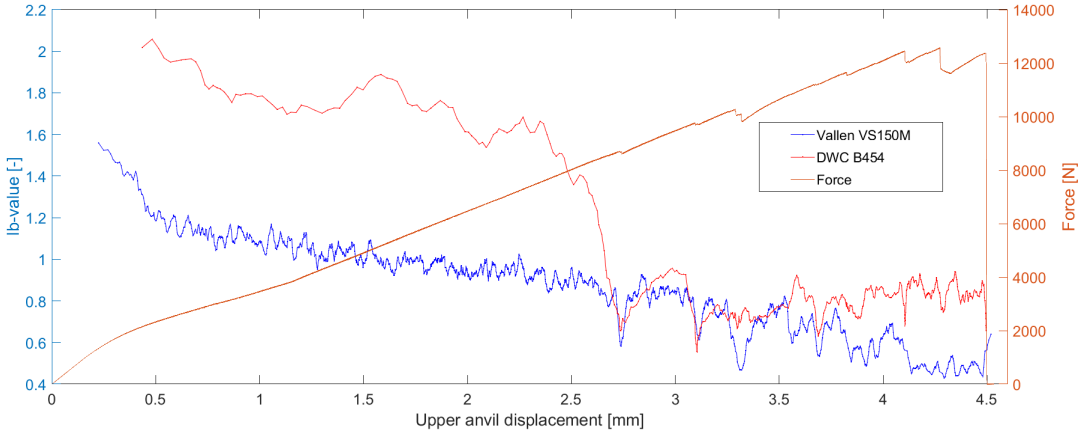

Fig. 6. Ib-value versus upper grip displacement: Vallen VS150M and DWC B454 datasets

200 samples, while these segments share the 50 samples overlap. The Ib-value curves were additionally treated with moving mean filter (10 samples). As can be seen, the results from both datasets are somewhat different in terms of the trend. However, even so it is possible to find there some signs of similar behavior, which is especially true in the events of sudden force drops. Under these circumstances, it is possible to observe a slightly higher sensitivity to the given phenomenon in the case of the VS150M sensor, even though it shows a more monotonous curve compared to DWC B454 result. The generally higher sensitivity of the VS 150 M sensor compared to the DWC 454 sensor is naturally due to the construction of the sensor itself, which, on the other hand, does not provide resolution in the area of the signal frequency spectrum.

On the other hand, if we take into account the overall nature of the Ib-value curves for both sensors, the DWC B454 curve provides a much better response related to the current state of the structural integrity, which is especially evident after reaching the upper grip displacement of 2.5 mm when there is a rapid decrease in the exponent but without a visible force drop. An explanation of such behavior can be found if we perform an Ib-value analysis on the DWC B454 dataset that has been filtered using the peak frequency for individual failure mechanisms (Fig. 7).

Between the upper grip displacement value of 2 mm and 2.5 mm are we noticing a rapid development of matrix cracking followed by delamination and fiber/matrix debonding, where the more extensive fiber break occurs after reaching 3.4 mm of the upper grip displacement. Subsequently, it is possible to register extremely low values of the exponent for all three dominant mechanisms up to the rupture itself. The only mechanism, which cannot be assessed due to the small number of detected AE hits is fiber pull-out.

4. Conclusions

In this paper, we dealt with the application of methodology involving improved b-value analysis and clustering technique to perform a structural integrity assessment of CFRP samples during the tensile test. The methodology consisted of the application of Ib-value technique on filtered dataset (according to peak frequency) of wideband AE sensor including further comparison with ones where Ib-value technique has been applied on the wideband/resonant AE sensor dataset without additional filtering. The obtained results indicate the ability to comprehensively evaluate the structural integrity status in terms of Ib-value exponent for individual failure mechanisms which makes it possible to reveal the extensive matrix cracking, fiber/matrix debonding or fiber failure.

It can be stated that in practice the proposed methodology would serve as an extension to conventional approaches, listed for example in the EN 15857 or ASTM E1067 standards, which stand out for their robustness and to a certain extent also for their general simplicity. However, as it was mentioned earlier, due to the fact that in real structures the real distance between the network of sensors and the position of the AE source is many times greater than in our case, it is also necessary to take into account the effect of the change in the frequency spectrum on the travelled distance of the wave, while we must not forget the influence of the sensor type, geometry of the tested structure or the material itself (number of layers, layout, fiber/matrix material properties). The mentioned factors therefore greatly influence the use of the peak frequency itself as a main parameter for the subsequent data evaluation process. For that reason, in real cases, it is necessary to choose a more robust parameter in the form of a weighted peak frequency or, alternatively, to perform a certain type of correction in the frequency spectrum area based on the detected position of the source, as in the case of distance corrected peak amplitude technique.

Acknowledgments

This work was supported by the project, Innovative and Additive Manufacturing Technology – New Technological Solutions for the 3D Printing of Metals and Composite Materials (CZ.02.1.01/0.0/0.0/17_049/0008407).

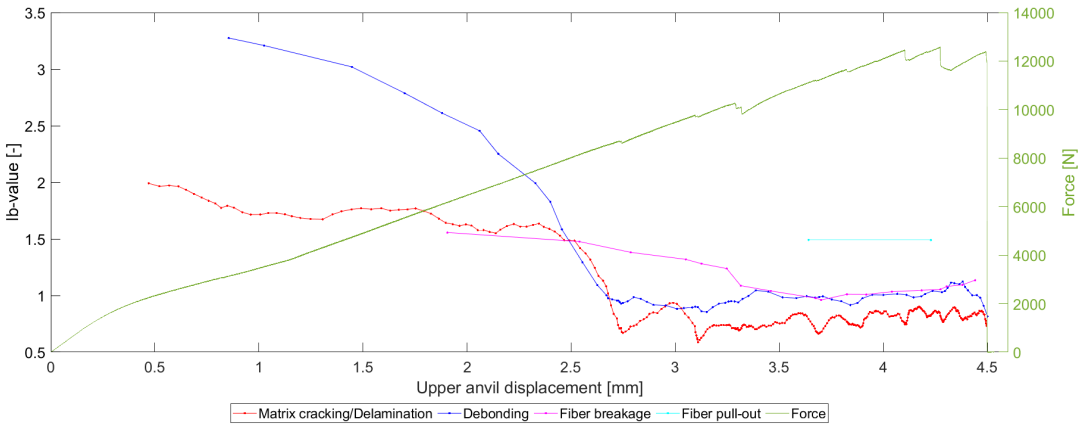

Fig. 7. Ib-value versus upper grip displacement: DWC B454 dataset filtered using peak frequency range for individual failure mechanisms

REFERENCES

[1] M. Šofer, J. Cienciala, M. Fusek, P. Pavlíček, R. Moravec, Materials **14**, 1-16 (2021). DOI: https://doi.org/10.3390/ma14040786

[2] J. Xu, W. Wang, Q. Han, X. Liu, Compos. Struct. **238**, 1-10 (2020). DOI: https://doi.org/10.1016/j.compstruct.2020.111948

[3] M. Šofer, P. Kučera, E. Mazancová, L. Krejčí, J. Nondestruct. Eval. **38**, 1-13 (2019). DOI: https://doi.org/10.1007/s10921-019-0627-0.

[4] P. Šofer, M. Šofer, J. Gebauer, P. Niegodajew, K. Gruszka, Acta Phys. Pol. A **138**, 272-275 (2020). DOI: https://doi.org/10.12693/APhysPolA.138.272.

[5] M. Šofer, P. Ferfecki, P. Šofer, Experimental construction of Lamb wave dispersion curves in plates, in: F. Trebuňa, R. Huňady, J. Bocko, J. Kostka, P. Frankovský, T. Kula (Eds.), 55th Conference on Experimental Stress Analysis (EAN 2017), Technical University of Kosice – Faculty of Mechanical Engineering (2017).

[6] M. Šofer, P: Ferfecki, P. Šofer, MATEC Web Conf. **157**, 08011 (2018). DOI: https://doi.org/10.1051/matecconf/201815708011

[7] M. Šofer, P. Šofer, P. Ferfecki, M. Molčan, J. Stryja, Appl. Math. Model. **89**, 413-427 (2021). DOI: https://doi.org/10.1016/j.apm.2020.08.017

[8] M. Shateri, M. Ghaib, D. Svecova, D. Thomson, Smart Mater. Struct. **26**, 1-17 (2017). DOI: https://doi.org/10.1088/1361-665X/aa6e43

[9] Ch.U. Grosse, M. Ohtsu, Acoustic emission testing, Springer, Berlin, Heidelberg (2008).

[10] M.G.R. Sause, In-situ monitoring of fiber-reinforced composites: theory, basic concepts, methods, and applications, Springer, Cham (2018).

[11] W. Roundi, A. El Mahi, A. El Gharad, J.-L. Rebiere, Appl. Acoust. **132**, 124-134 (2018). DOI: https://doi.org/10.1088/1742-6596/2125/1/012036

[12] D.Y. Jung, Y. Mizutani, A. Todoroki, Y. Suzuki, Open J. Compos. Mater. **7**, 117-129 (2017). DOI: https://doi.org/10.4236/ojcm.2017.73007

[13] M.V.M.S. Rao, K.J.P. Lakshmi, Curr. Sci. **89**, 1577-1582 (2005).

[14] B. Gutenberg, C.F. Richter, Seismicity of the Earth and Associated Phenomena, Princeton University Press, Princeton (1954).

[15] A.Y. Ng, M. Jordan, Y. Weiss, Adv. Neural Inf. Process. Syst. **14**, 849-856 (2001).

[16] https://www.mathworks.com/help/stats/spectralcluster.html, accessed: 17.04.2022

[17] X. He, D. Cai, P. Niyogi, Adv. Neural Inf. Process. Syst. **18**, 507-514 (2005).

[18] A. Ichenihi, W. Li, Y. Gao, Y. Rao, Appl. Acoust. **182**, 1-10 (2021). DOI: https://doi.org/10.1016/j.apacoust.2021.108184

[19] L. Kaufman, P.J. Rousseeuw, Finding groups in data: An introduction to cluster analysis, John Wiley & Sons, New Jersey (1990).

[20] S. Chaimontree, K. Atkinson, F. Coenen, Adv. Data Minining and App. 48-59 (2010). DOI: https://doi.org/10.1007/978-3-642-17316-5_5

[21] A. Loukidis, D. Triantis, I. Stavrakas, E.D. Pasiou, S.K. Kourkoulis, Mat Design Process Comm. 1-9. (2020), DOI: https://doi.org/10.1002/mdp2.176

[22] S. Colombo, I.G. Main, M.C. Forde, J. Mater. Civ. Eng. **15**, 280-286 (2003). DOI: https://doi.org/10.1061/(ASCE)0899-1561(2003)15:3(280)

[23] D. Jung, W.-R. Yu, W. Na, Compos. Commun. **22**, 1-8 (2020), DOI: https://doi.org/10.1016/j.coco.2020.100499

[24] M. Saeedifar, D. Zarouchas, Compos. B. Eng. **195**, 1-21 (2020). DOI: https://doi.org/10.1016/j.compositesb.2020.108039